

Published in final edited form as:

NMR Biomed. 2013 July ; 26(7): 860–871. doi:10.1002/nbm.2948.

***In vivo* MRI cell tracking using perfluorocarbon probes and fluorine-19 detection**

Eric T. Ahrens^{*} and **Jia Zhong**

Department of Biological Sciences and Pittsburgh NMR Center for Biomedical Research,
Carnegie Mellon University, Pittsburgh, PA, USA

Abstract

This article is a brief survey of preclinical *in vivo* cell tracking methods and applications using perfluorocarbon (PFC) probes and fluorine-19 (¹⁹F) MRI detection. Detection of the ¹⁹F signal offers high cell specificity and quantification abilities in spin-density weighted MR images. We discuss the compositions of matter, methods, and applications of PFC-based cell tracking using *ex vivo* and *in situ* PFC labeling in preclinical studies of inflammation and cellular therapeutics. We will also address potential applicability of ¹⁹F cell tracking to clinical trials.

Introduction

This article provides a brief survey of emerging methods and applications of MRI cell tracking using perfluorocarbon (PFC) based cell labels and fluorine-19 (¹⁹F) detection. Cells are the fundamental building blocks of any organ system. For small animal studies, there are many options available for tracking cells in their native environment, especially using various fluorescent and bioluminescent probes and reporters. However, there remains a great unmet need for cell tracking technologies that have the potential for clinical translation. There are several non-invasive diagnostic imaging modalities that are routinely used in humans including various radioisotope methods, MRI, computed tomography, and ultrasound. Adopting existing diagnostic imaging modalities to visualize cells in the body is a complex problem, but there is a strong rationale for undertaking this technical challenge. Non-invasive imaging of the dynamic trafficking patterns of populations of immune cells can play an important role in elucidating the basic pathogenesis of major diseases such as cancer and autoimmune disorders. Other cell populations, such as tumor or stem cells, can be tracked using MRI to provide insight into metastatic processes, cell engraftment and differentiation, and tissue renewal. Moreover, cells are increasingly being used as therapeutic agents to treat genetic and neurological disorders, as well as chronic conditions such as autoimmunity and cancer. A common need for virtually all cell therapies at the development stage is a non-invasive way to detect and quantify the cell biodistribution following injection. Non-invasive imaging of cell trafficking is capable of providing critical feedback regarding modes of action of the cells, optimal routes of delivery and therapeutic doses for individuals. On the regulatory side, emerging new therapies, such as those using immunotherapeutic and stem cells, are slow to gain regulatory approvals partly because clinical researchers are challenged to verify where the cells go immediately after inoculation and where they migrate to days and weeks later. Cell tracking can potentially provide this information and may help in lowering regulatory approval barriers.

^{*}Corresponding author: Eric T. Ahrens, Carnegie Mellon University, 4400 Fifth Avenue, Pittsburgh, PA 15213, eta@cmu.edu, (412) 268-5105 (voice), (412) 268-7083 (fax).

Intimately related to cell trafficking is inflammation and the inflammatory response. Biomedical research organizations commonly build research programs around major diseases where inflammation is a hallmark. Prevalent inflammatory diseases include, for example, arthritis, asthma, atherosclerosis, cancer, diabetes, chronic obstructive pulmonary disease (COPD), inflammatory bowel disease (IBD), infection, multiple sclerosis, and organ transplant rejection. The progression of these diseases can often be slow, and the effectiveness of treatment can be observed only after days, weeks or months. Thus, there is a strong unmet need for inflammation-specific diagnostics, as well as inflammation surrogate biomarkers that permit therapeutic developers to determine efficacy quickly, quantitatively, and in a longitudinal fashion. A related need entails pharmacological safety profiling to detect 'off target' inflammatory side effects in pre/clinical drug trials. A non-invasive, image-based biomarker could potentially fill these unmet needs. Vital imaging can accelerate the 'go/no go' decision making process at the preclinical and clinical trial stages, and can facilitate smaller, less costly trials by enrolling fewer patients. Imaging can potentially yield quantitative data about inflammation severity and time course in the anatomical context. The highest value imaging biomarker would have broad utility for multiple diseases and be applicable from mouse-to-man, thereby minimizing validation studies.

In an effort to devise next generation cell tracking probes, there has been significant recent interest in the use of ^{19}F -based cell labels employing PFC molecules. Detection of ^{19}F offers the advantage that there is no background signal from the host's tissues and only labeled cells are detected. Moreover, quantification of the PFC probe is directly related to the signal intensity in ^{19}F spin-density weighted MRI or magnetic resonance spectroscopy (MRS), thereby yielding a marker of the apparent number of cells in regions of interest, or alternatively, inflammation severity. The detection of PFC labeled cells using ^{19}F MRI/MRS is different from prior art using metal-ion-based contrast agents. In the case of the latter, one detects the presence of the paramagnetic contrast agent indirectly via its effect on T_1 , T_2 , and/or T_2^* of surrounding protons in mobile water. The PFC acts like a 'tracer' agent rather than a contrast agent since ^{19}F magnetic resonance directly detects the ^{19}F spins associated with the labeled cells.

Broadly, there are two approaches for labeling cells for tracking using PFC reagents. In the first approach, isolated cells of interest are labeled *ex vivo* (i.e., in culture) using a PFC formulated as an emulsion. Following transfer to the subject, cells are tracked using ^{19}F MRI/MRS (Fig. 1). The fluorine contained in the labeled cells yields cell-specific images, with no background, and these can be used to quantify apparent cell numbers at sites of accumulation. This approach, called '*in vivo* cytometry' (1) is capable of tracking a wide variety of cell types in a cell-specific manner. Alternatively, the cell biodistribution can be accurately measured in panels of intact tissue specimens using conventional high-resolution ^{19}F NMR spectroscopy measurements (1,2).

In the second approach, PFC emulsion is directly injected intravenously (i.v.). Following injection, the emulsion droplets are taken up by cells of the reticuloendothelial system (RES), including monocytes and macrophages. These '*in situ*' labeled leukocytes participate in inflammatory events resulting in ^{19}F accumulation at inflammatory loci. The ^{19}F MRI signal can be quantified by integrating the signal in regions of interest, and this integral is linearly proportional to the macrophage burden (3,4).

In this article we provide a brief survey of the compositions, methods, and applications of PFC-based cell tracking using *in vivo* cytometry and *in situ* cell labeling. We describe a sampling of applications in preclinical studies. We will also address potential applicability of ^{19}F cell tracking to clinical trials.

Perfluorocarbons

PFCs have been studied for more than 40 years and are among the most biologically inert organic molecules ever produced (5). There are no known enzymes that metabolize fluorocarbons *in vivo* (6), and they do not degrade at typical lysosomal pH values (7,8). These molecules contain C-F covalent bonds that are among the strongest known, a consequence of fluorine's high electronegativity. PFCs are generally highly hydrophobic and are often highly lipophobic. Consequently, PFCs have a tendency to segregate when placed in an aqueous environment and are immiscible in tissues; these property are partially responsible for PFCs being biological inert and nontoxic *in vivo* even at very high doses. Clearance of PFC agents from the body generally occurs via RES uptake and lung exhalation (9).

Most PFCs have the ability to readily dissolve oxygen, carbon dioxide and nitrogen. Early biological applications of PFCs exploited the high oxygen solubility (10). PFCs have been studied for decades as artificial oxygen transport vehicles and blood substitutes (11) for human use. Consequently, the safety profile of PFCs in man is well characterized.

The notion of using PFCs as a ^{19}F tracer agent has been around since the beginning of MRI/MRS (12–14). Early PFC imaging applications included their use as angiographic agents (12). There is strong rationale for ^{19}F MRI in certain applications because of fluorine's very low background biological abundance. Additionally, the ^{19}F isotope has 100% natural abundance and a spin- $\frac{1}{2}$ nucleus. The gyromagnetic ratio of ^{19}F differs from ^1H by only approximately 6% and has a relative sensitivity of 0.83. The sensitivity of PFCs as MRI reagents is highly dependent on its chemical structure. Optimal molecules should have a simple ^{19}F NMR spectrum, ideally having a single, narrow resonance to maximize sensitivity and minimize chemical shift image artifacts. Additionally, a short ^{19}F spin-lattice relaxation time (T_1) and a long spin-spin relaxation time (T_2) is desirable to promote rapid data acquisition times using conventional fast-imaging pulse sequences.

A review of suitable PFC molecules for ^{19}F MRI is described elsewhere (15,16). PFC molecular structures generally fall into several classes, including, branched, linear, cyclic and linear polyether. Perfluorooctyl bromide (PFOB), a linear PFC, was used early on as a ^{19}F MRI agent (17). PFOB is hydrophobic, but displays finite lipophilicity due to covalently-bound bromine, which enhances clearance rates from the body. The PFOB ^{19}F NMR spectrum has eight peaks, one for each CF_n moiety. To minimize chemical shift artifacts when using PFOB, MRI pulse sequences often incorporate pre-saturation RF pulses on undesired resonance peaks prior to readout. PFOB is of most PFCs used in biomedicine in that it displays multiple ^{19}F peaks, which significantly compromises sensitivity, as generally only one single peak can be used for imaging, and the other peaks must be suppressed. Interestingly, Giraudeau *et al.* (18) has described the use of frequency-selective refocusing pulses in multiple spin-echo sequence to suppress J-coupling between the CF_3 and CF_2 groups and associated signal loss, yielding a 4-to-6-fold increase in sensitivity over traditional gradient-echo (GRE) and chemical shift imaging (CSI) acquisitions. Significant improvement in MRI sensitivity can be achieved using the macrocyclic PFCs such as the perfluoro-15-crown-5 ether (PCE) molecule with 20 chemically equivalent fluorine atoms and a single NMR resonance. PFCs commonly used for MRI, such as PFOB and PCE, have intrinsically long T_1 relaxation times (e.g., >1 s) and this can limit the MRI data acquisition rate and ultimate sensitivity. More recently, linear perfluoropolyether (PFPE) polymers have been employed as a cell tracking reagent (1,19–21). The linear PFPE is sensitive due to its simple ^{19}F NMR spectrum (1,19,22) with a single major resonance, >40 chemically equivalent fluorine, and a small T_1/T_2 ratio (16). Moreover, linear PFPE has endgroups that are amenable to chemical modification to provide additional functionality, for example, to

enable covalent conjugation to bright fluorescent dye molecules for dual-modality detection (19).

Formulation of PFCs for cell tracking agents

PFCs are water insoluble and immiscible in cell membranes. Consequently, cell tracking applications require formulation of PFC into a biocompatible emulsion. A significant body of art on formulating stable PFC emulsions has been reported in the context of developing artificial blood substitutes (5,6,23). In these applications, emulsions must be stable in vascular circulation for extending periods of time, a property that is also desirable for *in situ* labeling of inflammatory macrophages for imaging. In contrast, *ex vivo* cell labeling demands alternative formulations that enable efficient and rapid intracellular uptake of PFC emulsion in culture media, including cells with an intrinsically-low phagocytic phenotype, such as stem cells and T cells.

Ideally, an emulsion for MRI cell tracking should have a small, uniform droplet size, ideally <200 nm. Large emulsion droplets can affect cell activation phenotype after labeling, for example in sensitive dendritic cells (DCs) (24). For *ex vivo* cell labeling, wash steps are employed to remove excess emulsion that is not taken up by cells after the labeling period; in the case of large emulsion droplets, the wash step is ineffective because centrifugation spins the emulsion down with the cells and excess emulsion cannot be discarded with the supernatant. Moreover, a tightly distributed droplet size of low dispersity helps ensure uniform labeling within a cell population.

A detailed description of the materials and methods associated PFC emulsion formulation for imaging applications is described elsewhere (16,25). Formulation generally employs surfactant(s) to stabilize the colloidal suspension and provide a practical shelf-life. Importantly, the choice of excipient may also alter biological characteristics of the emulsion, for example, to promote rapid uptake of PFC into cells in culture, or to enable a long circulation time in the blood stream.

Excipients may also be used to modify the ^{19}F NMR characteristics of the PFC molecules. For example, gadolinium chelates have been attached to the emulsion droplet surface to reduce the ^{19}F T_1 relaxation time, thereby imparting sensitivity enhancement by shortening data acquisition times (26). However, there is empirical evidence that the gadolinium chelate does not stay associated with the PFC emulsion droplet once inside the intracellular milieu (27).

Minimal excipient mass is desirable so that low amounts of MRI-inactive material is delivered inside the cell. Also, excipients should be non-toxic to cells and not modify phenotype, morphology or biological function of the labeled cells. Common emulsifiers include phospholipids (e.g., egg yolk phospholipids) and pluronics (e.g., poloxamer 188 or F68) (5). In one example, a 'self-delivering' and stable emulsion for *ex vivo* cell labeling was formulated using linear PFPE, pluronic F68 and linear short chain polyethylenimine (19). The formation of stable, small particle, colloidal suspensions of PFC and excipients requires high energy processing methods. Methods include, for example, high pressure, high shear homogenization (e.g., microfluidization) and sonication. The most common degradation mechanism for PFC emulsions is Ostwald ripening, a molecular diffusion phenomena that results in a gradual growth of the larger particles at the expense of smaller ones (28,29) and represents a major challenge in formulating stable PFC emulsions (30–32). Additional details describing emulsion formulations are described elsewhere (16).

There is increasing emphasis on non-invasive multi-modal imaging. Dual-mode PFC emulsions that can be detected by both ^{19}F and fluorescence have been described in several

studies (19,33–35) In preferred formulations, the PFC molecule is directly conjugated to a fluorescent dye prior to emulsification to ensure coincident MRI and fluorescence signals (Fig. 2) (19). Alternatively, lipophilic fluorescent dyes can be added to the surfactant when phospholipid-based excipients are employed (36). In preclinical studies, these dual-mode reagents enable one to positively identify the fate and phenotype of labeled cells following ^{19}F MRI, days and weeks after cell transfer using flow cytometry, fluorescence microscopy, and/or *in vivo* optical imaging (21). In one example, Janjic *et al.* (19) developed dual-mode PFC emulsions by direct conjugation of dye molecules in the visible spectral range to linear PFC and formulated a self-delivering emulsion for *ex vivo* cell labeling. A linear correlation was observed between the ^{19}F NMR signal and the fluorescence signal in labeled cells. Mouse primary T cells were labeled by the dual-mode PFC emulsion (Fig. 2a). *In vivo* ^{19}F imaging showed hot-spots in multiple lymph nodes, which was validated by fluorescence detection via optical microscopy of CD4+ cells in the isolated lymph nodes and by flow cytometry (Fig. 2b). Near-infrared dyes have also been incorporated into PFC emulsions enabling *in vivo* imaging at moderate tissue depths (37). Moreover, fluorescent PFC emulsions have stand-alone utility as an optical-only cell labeling probe due to their brightness, low toxicity, long retention time in cells, and the existence of self-delivering formulations.

***In vivo* cytometry**

One of the longstanding goals in the field of cellular and molecular MRI is targeted imaging of cells of a particular phenotype *in vivo*. This goal is often stymied by the fact that MRI is intrinsically insensitive compared to other techniques (e.g., positron emission tomography, PET). Targeting cellular epitopes *in situ* with an MRI probe requires overcoming the quadruple requirements of efficient tissue access of the imaging probe following intravenous injection, high binding specificity, high cellular epitope density, and high payload of the MRI-detectable moiety (38,39). However, in many instances, one can sidestep these limitations using *ex vivo* cell labeling, where one optimally labels cell populations of interest that have been pre-sorted for the desired phenotype in culture, followed by (re)introduction of the labeled cells into the subject. This approach is particularly feasible for cellular therapies that are already routinely cultured outside the body prior to infusion into the patient; a cell labeling reagent can be just another ‘factor’ that is added to cells prior to injection. Other cell types, such as autologous leukocytes obtained from peripheral blood leukapheresis procedures, bone marrow harvests, cells recovered from tissue biopsies, or cell lines, are also amenable to *ex vivo* cell labeling for MRI. Although ^{19}F MRI has been around for decades (15), the notion of using PFCs for cell tracking and quantification in a cell-specific manner, i.e., *in vivo* cytometry, is a recent development. *Ex vivo* ^{19}F cell labeling, was first proposed in 2005 (36). The fluorine contained in the labeled cells yields cell-specific images, with no background, that can be used to quantify apparent cell numbers at sites of accumulation.

In vivo cytometry was first used to visualize dendritic cells (DCs) in mouse (36) (Fig. 1a). Several T cell studies have used ^{19}F cell tracking to examine early inflammatory events in a rodent model of type-1 diabetes (1) (Fig. 1b), an acute inflammation model (21), and the biodistribution of Muc1-specific lymphocytes in inflammatory bowel disease (IBD) (2). Other studies have employed ^{19}F MRI cell tracking to visualize stem cells *in vivo* in rodent models (Fig. 1c) (33,40–42). The use of PFC labeling for cancer cells has also been reported (43). Additionally, primary human DCs relevant to immunotherapeutic clinical trials have been labeled with PFC, biologically characterized, and imaged in an immune compromised mouse (44).

While certain cells having a phagocytic phenotype, such as immature DCs, readily take up PFC emulsion droplets in culture, other non-phagocytic cell types such as stem cells and T cells, do not. For the latter cell types, transfection methods are needed, for example, by employing a premix step of the emulsion with a cationic transfection agent prior to addition to the cell culture (36). However, transfection agents are sometimes toxic to sensitive cell types such as primary lymphocytes, can alter cellular phenotype, and often not suitable for use in human health. An important PFC reagent innovation has been the development of self-delivering emulsion formulations that do not require the use of a transfection agent and a premix step (19) and results in overall improvements in cell viability and ease of use. Current formulations of PFC reagents can efficiently label cells by simple co-incubation over a period of several hours. The degree of labeling can readily be assayed by acquiring a ^{19}F NMR spectrum of a sample consisting of a cell pellet of known cell number and a fluorine reference compound with a disparate chemical shift, where the mean ^{19}F /cell is calculated from the integrated areas of the PFC and reference peaks (1). This simple assay method commonly yields cell loading values ranging from 10^{11} to 10^{13} ^{19}F /cell (19).

The PFC emulsions used for *ex vivo* cell labeling have been rigorously tested and appear to be biologically safe, presenting no observed adverse effects to viability or function in cells. Numerous studies have investigated the impact of PFC cell labeling on cellular phenotype and function in primary immune cells using a variety of sensitive *in vitro* assays, for example in the context of murine DCs (36), T cells (21), and stem cells (33,40–42). The most detailed *in vitro* study to date involved PFC labeled primary human DCs (44); cells were assayed for viability, maturation phenotype, cytokine production, T cell stimulatory capacity, and chemotaxis (44), and no difference in these parameters was observed between labeled and unlabeled cells. More recently, primary human CD34+ hematopoietic stem cells were labeled with PFC and shown to retain their pluripotency and ability to reconstitute the full leukocyte repertoire *in vivo* in mice that underwent immunoablation (45).

In PFC labeled cells having a mitotic phenotype, cell division and subsequent dilution of the intracellular label, can potentially limit long-term cell tracking studies of itinerant cells and/or decrease the accuracy of cell quantification. Death of labeled cells can lead to dispersion of the reagent and loss of ^{19}F signal. Potentially, the PFC droplets can also be transferred to resident phagocytes (e.g., macrophages). If a large number of these labeled phagocytes remain in a region of interest, false positive signals could result. These caveats are the same for many commonly used imaging modalities where a tracer material is utilized, for example with SPECT using Indium-111 probes and with various nanoparticle probes (SPIO, NIR, Q-Dots, etc.). To rigorously overcome detection of false positive results from live versus dead cells, a genetically-encoded reporter gene may be employed, for example for MRI, using the ferritin gene (46–48) or a CEST-type agent (49) which are degraded by proteolytic enzymes upon cell death.

NMR cytometry

In many instances, a key question that arises in the early development of cell therapies is the cell biodistribution post-transfer. NMR of fixed tissue samples is an alternative method to detect and quantitate *ex vivo* labeled cells (1,2), and has the advantage of high sensitivity. A quantitative cell biodistribution assay can be used to characterize delivery efficacy, cell engraftment, and possible off-target cellular niches. Conventional methods to assay cell biodistribution in excised tissue panels, such as histology and flow cytometry of single cell suspensions, represent a laborious obstacle toward gaining this information that lacks quantitative rigor. Alternative methods may rely on the use of radioisotopes to label cells prior to infusion. However, radioisotope labeling may cause changes to cell function, especially to those cells that are exquisitely sensitive to irradiation such as stem cells (50).

Moreover, the radioisotope lifetime may limit long-term cell detection and quantification (51,52).

Excised tissue samples containing PFC labeled cells can readily be assayed using NMR. Tissue panel preparation involves fixation, weighing, and the acquisition of 1-dimensional ^{19}F spectra. An aliquot of a ^{19}F reference solution (e.g., trifluoroacetic acid) is generally added to the tissue specimen, preferably placed in a small sealed capillary alongside the tissue mass. The tissue specimen plus reference solution should fit entirely within the receptive field of the NMR coil (~1–2 cm along the z-axis) in order to detect every ^{19}F spin for accurate quantification. This sample preparation may degrade the spectral linewidth compared to conventional high-resolution NMR practices, but as only the integrated peak area is used and the spectrum is simple, linewidth is of limited concern. The total number of cells in the tissue sample is calculated from knowledge of the ^{19}F /cell following labeling (described above), the integral of the ^{19}F spectrum of the tissue sample, and the integral of a fluorine reference compound added to the NMR tube (3). Normalization of the measured cells/sample by the specimen weight yields the average tissue cell density. In preferred implementations of these methods, a 10 mm broadband probe is used. For example, in murine studies a 10 mm NMR tube can accommodate any intact organ (e.g., liver and brain) without the need for manual segmentation. If tissue panels involved large numbers of samples, commercially-available robotic or automated NMR sample changers can be employed to accelerate measurement throughput. The PFC compounds are stable over time, thus the samples can be safely stored until the time of measurement or shipped to appropriate instrumentation without loss of measurement accuracy. As the NMR tissue preparation and measurement is non-destructive, the same tissues can be processed for histology to refine the tissue analysis as required.

Inflammation and *in situ* PFC cell labeling of macrophages

Inflammation is a protective mechanism initiated by the immune system to remove foreign pathogens or injurious stimuli and start the healing process. Cascades of biological events are involved in an inflammatory response, which includes but not limited to recognition of pathogen, activation of immune cells, and secretion of inflammatory mediators (53). As a consequence of these events, there is often recruitment and translocation of leukocytes from circulation to sites of inflammatory loci. *In vivo* visualization of inflammatory hot-spots advances our understanding of the inflammatory response, provides significant diagnostic value for a wide range of diseases, and can be used as a surrogate marker to monitor therapeutic interventions.

Following systemic PFC administration to a subject, emulsion droplets are initially taken up *in situ* by circulating phagocytes in the blood stream. These cells are a subgroup of leukocytes that include primarily monocytes, macrophages, neutrophils, and DCs; these cell types are tasked with engulfing and removing cellular debris, foreign substances, and pathogens. Macrophages are monocytes in their matured form, and these cells preferentially engulf PFC emulsion *in situ* (54). To a much smaller degree, other cells types, including neutrophils (55,56), DCs, B lymphocytes (57), microglia (58) can also uptake PFC *in situ*.

The fluorine-tagged leukocytes participate in inflammatory events *in vivo*. When labeled cells accumulate in sufficient amounts at sites of inflammation, they become detectable by ^{19}F MRI. *In situ* labeling has been widely used for ^{19}F MRI of phagocytes in a multitude of preclinical models of human disease (3,4,13,34,55–57,59–64). Unlike *in vivo* cytometry, *in situ* labeling of leukocytes with PFC emulsion has the advantage that it does not require procedures to collect immune cells, handle them *ex vivo* and reintroduce them back into the subject. *In situ* labeling has the disadvantage that the precise phenotype of labeled cells is

unknown and may involve multiple cell types. Also, the amount of ^{19}F /cell taken up by cells *in situ* is not known, thereby hindering cell quantification *in vivo*. However, inflammation quantification in spin-density weighted images can be performed and involves counting the number of apparent fluorine atoms in regions of interest, with aid of a calibrated ^{19}F reference (e.g., capillary filled with PFC) placed alongside the subject in the field of view. The number of fluorine atoms present in regions of interest is approximately linearly proportional to the macrophage burden (3,4).

The notion of using *in situ* PFC cell labeling and ^{19}F MRI to detect inflammation has been around since the first demonstration of ^{19}F MRI. Early ^{19}F MRI studies visualized ^{19}F hot-spots in rat liver, tumor, and abscess following PFC infusion (13). In other studies (64), PFOB was administered intravenously to a mouse that received abdominal radiation, and a decreased ^{19}F uptake was detected in the spleen indicating impaired phagocytic function of resident macrophages as a consequence of acute radiation damage (64). Ratner *et al.* (63) detected ^{19}F signal accumulation in a mouse tumor after intravenous delivery of PFOB, presumable due to tumor-associated macrophages. In the late 1990's, ^{19}F MRI with *in situ* cell labeling was used to monitor inflammation associated with autoimmune disease in the context of experimental allergic encephalomyelitis (EAE), an animal model of multiple sclerosis (62). In these experiments, perfluoro-15-crown-5 ether (PCE) emulsion was infused into EAE rats, and macrophage recruitment was detected in the tissue in proximity to the midbrain, medulla, and the cervical spinal cord.

More recently, *in situ* PFC labeling has been applied to a broad spectrum of inflammatory disorders in animal models [for recent reviews see (65,66)]. Flögel and colleagues (57) reported macrophage visualization in ischemia models of the myocardium and cerebrum following intravenous PCE emulsion infusion. Ebner *et al.* (56) reported monocyte/macrophage trafficking into sites of lipopolysaccharide-induced pulmonary inflammation and described a strong correlation between the intensity of ^{19}F signal and the severity of lung inflammation (56). Hertlein *et al.* (55) reported the trafficking of phagocytic cells to the murine thigh as part of a bacteria-induced host immune response (Fig. 3). Longitudinal image comparisons were made using both PFC emulsion and iron-oxide nanoparticles in the same model. It was shown that PFC could delineate abscess boundaries in both the acute and chronic phases, but iron-oxide was not able to clearly define the lesion in the acute phase. In another study (60), a neuroinflammatory response was visualized in the peripheral nervous system using a lysolecithin injection into the rat sciatic nerve. Following PFC injection, macrophage recruitment was observed focally at sciatic nerve lesions. In other studies (59), a rodent collagen-induced rheumatoid arthritis model was used to show a strong correlation between disease severity, as observed by quantification of ^{19}F uptake in affected limbs, and conventional joint caliper measurements. To modulate disease severity, glucocorticoid therapy was administered to the rodents.

Non-invasive visualization of the inflammatory response associated with organ transplant rejection is potentially a key use of PFC and MRI, as there is a strong motivation to supplant invasive 'gold-standard' biopsy procedures. Potentially, the magnitude of ^{19}F signal in the rejecting organ scales with organ rejection stage. Several studies (34,61) applied *in situ* PFC labeling to image organ rejection. Hitchens *et al.* (34) quantified the ^{19}F signal in rat heart and kidney allograft rejection models and showed that the patterns of signal corresponded to rejection histopathology (Fig. 4). Comparisons with the use of iron-oxide nanoparticles were also performed in the same models. Hitchens reported that both labeling methods showed strong correlation between MRI signal and the graft rejection status. However, the complex hypointensity patterns in T_2^* -weighted images hinders unambiguous detection of iron-labeled cells and complicates the process of rejection quantification and scoring. In another study, Flögel and colleagues showed quantitative analysis of ^{19}F signals is more sensitive to

rejection in the early stage than conventional makers such as ^1H anatomical images, functional MRI scans, or palpation scores (61).

Inflammatory bowel disease (IBD) has also been the subject of *in situ* PFC labeling studies. Kadayakkara *et al.* (4) showed that macrophage activity associated with IBD in a $\text{IL-10}^{-/-}$ mouse model can be non-invasively detected and scored using ^{19}F MRI. The bowel is notoriously difficult to image using conventional ^1H due to the complexity of the background contrast and 3D anatomy. In this study, the 3D patchy inflammation was imaged in an 8 minute acquisition time (Fig. 5). Validation studies used immunofluorescence, qRT-PCR and *in situ* macrophage ablation, to demonstrate that the PFC was localized within macrophages and that the cell quantity was reflected in the magnitude of the colon ^{19}F signal. Additionally, the impact of putative therapeutics used to treat colitis was reflected in the magnitude of the ^{19}F signal measured *in vivo*.

As described above (see ‘NMR cytometry’), conventional liquid-state NMR instrumentation can also be used to rapidly and quantitatively assay inflammation in intact, excised tissue samples. Discovery and preclinical studies often rely on histological analysis of a panel of tissues to examine the extent of inflammation, and these procedures are often viewed as time consuming, expensive, and a bottleneck in research and development. As an example of the applicability of NMR methods, Ahrens *et al.* (3) used a rat model of EAE displaying pronounced CNS inflammation. This study manually segmented the fixed rat brain and spinal cord into 15 segments and subjected the intact tissue samples to ^{19}F NMR analysis. The results displayed the inflammation profile along the entire length of the CNS. The results for each sample were expressed as the ‘inflammatory index’ with units of fluorine atoms per tissue weight, which was shown to be proportional to the macrophage burden via PCR analysis. Overall, ^{19}F NMR can be used to dramatically reduce the time to evaluate macrophage involvement in a wide variety of acute and chronic inflammatory models. Importantly, liquid-state NMR spectrometers that are ^{19}F -capable are ubiquitous in laboratory research centers, thus these methods can be widely utilized for inflammation research.

Sensitivity

Fluorine-based cell tracking directly detects the density of ^{19}F spins associated with labeled cells, which is generally dilute compared to ^1H in biological tissue. Importantly, ^{19}F cell tracking does not demand a high ^{19}F signal-to-noise ratio (SNR). Because there is negligible ^{19}F background, any ^{19}F signal detected is from labeled cells. Unlike ^1H anatomical imaging, where one relies on its high SNR to resolve anatomical detail and organ definition, the ^{19}F image only needs to display localized ‘pools’ of cells at low SNR (e.g., <5) and low resolution; the high-resolution ^1H underlay provides the detailed anatomical context.

From *ex vivo* labeling studies, the amount of ^{19}F loaded in cells typical ranges from approximately 10^{11} to 10^{13} ^{19}F /cell (19); we speculate that the degree of labeling reported for a given cell type correlates to the overall cell (or cytoplasmic) volume. Given this cell labeling level, it has been shown empirically that the minimum cell detection sensitivity for ^{19}F cell tracking is on the order of 10^4 to 10^5 cells per voxel for clinical MRI systems and 10^3 – 10^4 cells per voxel for high-field animal scanners (1,36,41,42,67). Single-voxel *in vivo* magnetic resonance spectroscopy (MRS) detection is expected to yield even higher sensitivity to sparse cell numbers. For cell detection in fixed samples using liquid-state NMR spectrometers, cell detection sensitivity is even greater, approaching $<10^3$ cells per sample (unpublished). Experimental details, such as the ^{19}F T_1/T_2 ratio of the PFC used, the number of NMR peaks of the PFC molecule, the cell type (i.e., cell size) labeled, image

acquisition methods, magnetic field strength, and RF coil configuration determine the actual sensitivity possible for a particular study.

MR Methods

Most small animal MRI scanners can readily be adapted to image ^{19}F with the addition of a suitable $^{19}\text{F}/^1\text{H}$ coil, and numerous vendors can supply such a coil. The preferred RF coil configurations for multi-nuclear MRI are discussed elsewhere (68–71). Clinical scanners are generally designed to be more specialized for ^1H -only applications, but most can be adapted to scan ^{19}F with the addition of a $^{19}\text{F}/^1\text{H}$ coil. However, some scanners will also require an aftermarket preamplifier, T/R switch and RF power amplifier suitable for ^{19}F . Additionally, clinical ^{19}F MRI practitioners may require a vendor-supplied research license to use/install multi-nuclear imaging capabilities.

Pulse sequences with an intrinsically-high SNR per image acquisition time are generally preferred, such as RARE (56,57), SSFP (14,55), GRE (72,73), and EPI (74,75). These sequences may be combined with parallel imaging techniques (76,77) to further reduce the total imaging acquisition time.

In the future, there is likely to be significant opportunities to improve the data acquisition schemes used to acquire ^{19}F data sets that will greatly accelerate the acquisition speed and cell detectability. To date, ^{19}F cell tracking studies have mostly used conventional pulse sequences (spin-echo, RARE, GRE, etc.) that do not exploit the unique characteristics of the ^{19}F data. The ^{19}F signal appears as isolated pools of signal from cell deposits against a background of pure noise. Generally, the image field of view contains only ‘sparse’ data, where often only a few percent of voxels of the total contain signal. Additionally, the ^{19}F spin-density weighted images are generally devoid of structural information and have minimal high-frequency spatial components; the ^1H image underlay provides the anatomical context. Due to the low SNR, long MRI scan times may be required using conventional pulse sequences that may hinder the use of ^{19}F detection in regions of sparse cell numbers or to detect low-grade inflammation.

Recently, compressed sensing (CS) methods (78–83) have been used to reduce MRI scan times in situations where images are expected to contain ‘information-sparse’ features. In CS, k-space is undersampled below the Nyquist criteria and image reconstruction constraints are customized for each application. CS is a 3D imaging approach that can improve the image SNR per unit acquisition time and therefore enhance the ability of ^{19}F cell tracking to detect sparse cell numbers by enabling increased signal averaging within the temporal confines of an imaging session. A recent CS MRI study (84) in the context of ^{19}F cell tracking showed that the method is effective in significantly reducing the image acquisition time by at least 8-fold without seriously effecting image features and ^{19}F spin quantification accuracy (Fig. 6). Our view is that data acquisitions schemes that have reduced k-space sampling (e.g., CS) will be important for future clinical applications of ^{19}F based cell tracking as a means to minimize scan time.

One of the characteristics of ^{19}F cell tracking is that the resulting images can be quantified by integrating the signal hot-spots in spin-density weighted images. Often an external ^{19}F reference standard is used with the scans in the image field of view to provide absolute quantification of the total number of fluorine atoms present in regions of interest. Several factors can affect the accuracy of these integrated signal values. Noise in complex images is normally distributed about zero independently for both the real and imaginary components in each voxel. Because the ^{19}F images are often in the low SNR regime, converting the complex-valued images to magnitude images, which is commonplace in MRI, creates non-normally distributed noise having a Rician distribution (85). Consequently, magnitude

images have a non-zero mean pixel value in regions devoid of signal, which introduces a noise-dependent bias to the data when the SNR is low. Thus, ideally one should compensate for the Rician bias by rescaling magnitude intensity values that are close to zero (21,85).

Motion of the subject during the ^{19}F scan is another potential source of ^{19}F quantification inaccuracy. As with ^1H scans, the sensitivity of ^{19}F images to motion is dependent on the particular imaging method used. Sequences such as UTE (86), SWIFT (87) or other acquisition scheme (88) are preferred for minimizing motion-related quantification inaccuracies. Several studies have addressed motion correction for ^{19}F imaging based on simultaneous proton scans (73) and/or proton self-navigation techniques (89).

Another practical concern relates to the use of gaseous anesthesia for animal MRI experiments. Gaseous anesthesia is generally fluorinated, and potentially false positive ^{19}F signals may appear over time if the anesthesia accumulates in tissue. Our experience is that a faint and diffuse ^{19}F MRI signal may appear predominantly in subcutaneous fat regions after extended periods (>2 hour) under gaseous anesthesia. However, in practice, the use of fluorinated anesthesia gases does not cause a serious roadblock for ^{19}F cell tracking. The ^{19}F images should be acquired near the beginning of the imaging session, and if significant signal averaging is employed, one can acquire the center portion of k-space first to minimize any potential ^{19}F signal contamination from the anesthetic. However, to rigorously avoid potential false positive ^{19}F signals from gaseous anesthesia, an option is to use injectable liquid anesthesia, for example, delivered via a mechanical pump and an intraperitoneal catheter (1,36) for the duration of the scanning session.

PFC as an intracellular oxygen sensor

In addition to cell tracking capabilities, PFC cell labels can also be used as intracellular oximetry probes. *In vivo* measurement of intracellular oxygen level facilitates our understanding of cell physiology and its response to therapeutic procedures. PFC is known to dissolve paramagnetic oxygen, thereby decreasing the ^{19}F T_1 and T_2 (75,90,91). Normally T_1 is used to measure the partial pressure of oxygen ($p\text{O}_2$), as it exhibits a larger response to O_2 concentration compared to T_2 . The ^{19}F relaxation rates of PFC exhibit a highly linear dependence with local oxygen levels in proximity to emulsion droplets. Oxygenation *in vivo* can be calculated using an *in vitro* calibration curve correlating NMR relaxation rates with absolute $p\text{O}_2$ (92). Compared to traditional oxygen sensing approaches using probe electrodes or ESR (93), ^{19}F MRI oximetry has minimal invasiveness, can be applied longitudinally, and is suitable for deep-seated cell populations.

Much of the work using PFC oximetry focuses on cancerous tissue (94). For example, in prior tumor studies, the PCE emulsion was introduced i.v., or injected directly intratumorally (75,94–99). For i.v. delivery, generally a large PFC dose is injected systemically, and a small fraction of the PFC accumulates at the tumor site, which may be visible several days post-administration. The PFC emulsion droplets are sequestered predominantly in the periphery of the tumors because of leakage in tumor vasculature (98,99), or phagocytosed by tumor-associated macrophages (75,97). Generally, in the above routes of administration PCE emulsion deposits are distributed very non-uniformly in the tumors.

More recent studies (43) have shown that it is feasible to measure intracellular $p\text{O}_2$ in a cell-specific manner using *in vivo* cytometry methods. Kadayakkara *et al.* (43) investigated PFC labeled 9L glioma cells implanted into the rat striatum. Following inoculation of labeled 9L cells into the striatum, tumor cells were imaged using ^{19}F MRI (Fig. 9a). Single voxel ^{19}F MRS was used to longitudinally measured the mean intracellular $p\text{O}_2$ in the tumor implant

(43). The same study then monitors changes in pO_2 before and after treatment with the chemotherapeutic agent bis-chloroethylnitrosourea (BCNU) (Fig. 9b). A single BCNU dose was sufficient to produce a dramatic and sustained increase in tumor pO_2 (Fig. 9b). At the experimental endpoint, histology was used to confirm that the PCE was retained intracellularly in 9L cells via a dual-mode version of the labeling emulsion and fluorescence microscopy (see Ref. (43)); no obvious extracellular PCE could be observed. These data show that intracellular oxygen sensing is feasible in a cell specific manner, with high sensitivity.

Prospects for clinical translation

The use of ^{19}F cell tracking in clinical trials is still in its infancy. Our view is that in the future *in vivo* cell tracking will routinely be used to provide a surrogate biomarker for cellular therapeutic clinical trials and for inflammation detection and monitoring, in combination with drug trials. Various types of perfluorocarbons have long been contemplated as oxygen carriers in traumatic surgeries and as artificial blood substitutes (100), and thus a large volume of data exists on the toxicity profile and clearance pathways of this class of molecules. Importantly, in using these products large doses of the PFC are delivered systemically in an effort to maintain satisfactory tissue oxygen levels. In the case of *in vivo* cytometry, a relatively miniscule quantity of PFC, contained within the transferred cells, is delivered to the subject suggesting that PFC cell tracking will be highly safe for human use. Thus, in these applications the imaging agent may be considered as an excipient to the cell therapeutic, and presumably lower regulatory hurdles are present. In the case of *in situ* labeling, a much larger PFC dose must be delivered to the subject, thus there are elevated safety concerns. The technical barriers associated with implementation of ^{19}F MRI/MRS on a clinical scanner are surmountable. Prior studies using ^{19}F MRI on a clinical scanner have demonstrated the feasibility of noninvasive characterization of PFC signal intensity at clinical field strength. (69,73,101)

Conclusions

Overall, ^{19}F MRI cell tracking using PFC tracer agents is a rapidly emerging alternative to 1H -based approaches using metal-ion-based contrast agents. Future improvements in sensitivity and functionality of ^{19}F -based cell tracking will require an integrated and interdisciplinary approach that rigorously applies principles of chemistry, biology, spin physics, and image processing. Our view is that these technical undertakings are worthwhile, as work in this field to date has shown that this sub-field of MRI cell tracking can produce unique information about cellular processes *in vivo* in a diverse range of applications.

Acknowledgments

We thank Dr. Kevin Hitchens for review of the manuscript. We acknowledge support from the National Institutes of Health grant R01-CA134633, the Pittsburgh NMR Center for Biomedical Research, supported by P41-EB001977, and the Dana Foundation.

Abbreviation List

BCNU	bis-chloroethylnitrosourea
CEST	chemical exchange saturation transfer
CSI	chemical shift imaging
COPD	chronic obstructive pulmonary disease

CS	compressed sensing
DC	dendritic cell
EPI	echo planar imaging
ESR	electron spin resonance
¹⁹F	fluorine-19
IBD	inflammatory bowel disease
GRE	gradient-echo
MRI	magnetic resonance imaging
MRS	magnetic resonance spectroscopy
NIR	near-infrared
NMR	nuclear magnetic resonance
PCE	perfluoro-15-crown-5 ether
PFC	perfluorocarbon
PFOB	perfluorooctyl bromide
PFPE	perfluoropolyether
PET	positron emission tomography
RARE	rapid acquisition with refocused echoes
RES	reticuloendothelial system
SNR	signal-to-noise ratio
SSFP	steady-state free precession
SPIO	superparamagnetic iron oxide
SWIFT	sweep imaging with Fourier transform
3D	three-dimensional
UTE	ultrashort echo time

References

1. Srinivas M, Morel PA, Ernst LA, Laidlaw DH, Ahrens ET. Fluorine-19 MRI for visualization and quantification of cell migration in a diabetes model. *Magn Reson Med*. 2007; 58(4):725–734. [PubMed: 17899609]
2. Kadayakkara DK, Beatty PL, Turner MS, Janjic JM, Ahrens ET, Finn OJ. Inflammation driven by overexpression of the hypoglycosylated abnormal mucin 1 (MUC1) links inflammatory bowel disease and pancreatitis. *Pancreas*. 2010; 39(4):510–515. [PubMed: 20084048]
3. Ahrens ET, Young WB, Xu H, Pusateri LK. Rapid quantification of inflammation in tissue samples using perfluorocarbon emulsion and fluorine-19 nuclear magnetic resonance. *Biotechniques*. 2011; 50(4):229–234. [PubMed: 21548906]
4. Kadayakkara DK, Ranganathan S, Young WB, Ahrens ET. Assaying macrophage activity in a murine model of inflammatory bowel disease using fluorine-19 MRI. *Lab Invest*. 2012; 92(4):636–645. [PubMed: 22330343]
5. Riess JG. Oxygen carriers (“blood substitutes”) - Raison d’etre, chemistry, and some physiology. *Chem Rev*. 2001; 101(9):2797–2919. [PubMed: 11749396]

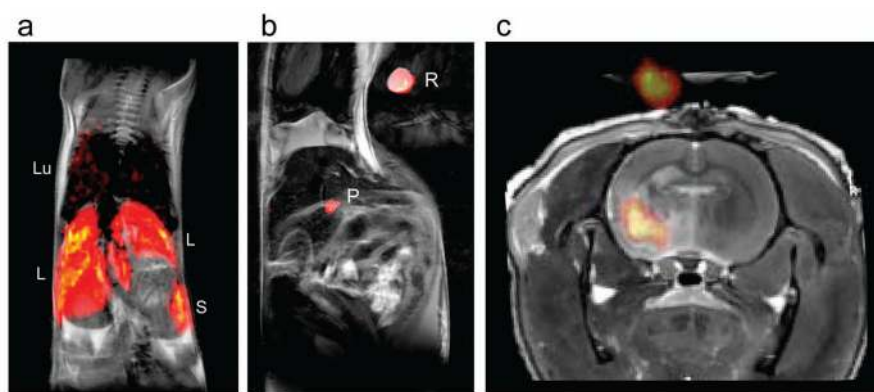
6. Krafft MP, Riess JG. Perfluorocarbons: Life sciences and biomedical uses dedicated to the memory of professor guy Ourisson, a true renaissance man. *J Polym Sci, Part A: Polym Chem*. 2007; 45(7): 1185–1198.
7. Krafft MP, Chittofrati A, Riess JG. Emulsions and microemulsions with a fluorocarbon phase. *Curr Opin Colloid Interface Sci*. 2003; 8(3):251–258.
8. Krafft MP. Fluorocarbons and fluorinated amphiphiles in drug delivery and biomedical research. *Adv Drug Deliv Rev*. 2001; 47(2–3):209–228. [PubMed: 11311993]
9. Castro O, Nesbitt AE, Lyles D. Effect of a perfluorocarbon emulsion (fluosol-da) on reticuloendothelial system clearance function. *Am J Hematol*. 1984; 16(1):15–21. [PubMed: 6695906]
10. Clark LC, Gollan F. Survival of mammals breathing organic liquids equilibrated with oxygen at atmospheric pressure. *Science*. 1966; 152(3730):1755. [PubMed: 5938414]
11. Spahn D, Kocian R. Artificial O₂ carriers: status in 2005. *Curr Pharm Des*. 2005; 11(31):4099–4114. [PubMed: 16378514]
12. Joseph PM, Yuasa Y, Kundel HL, Mukherji B, Sloviter HA. Magnetic resonance imaging of fluorine in rats infused with artificial blood. *Invest Radiol*. 1985; 20(5):504–509. [PubMed: 4044195]
13. Longmaid HE 3rd, Adams DF, Neirinckx RD, Harrison CG, Brunner P, Seltzer SE, Davis MA, Neuringer L, Geyer RP. In vivo ¹⁹F NMR imaging of liver, tumor, and abscess in rats. Preliminary results *Invest Radiol*. 1985; 20(2):141–145.
14. Holland GN, Bottomley PA, Hinshaw WS. F-19 Magnetic-Resonance Imaging. *J Magn Reson*. 1977; 28(1):133–136.
15. Ruiz-Cabello J, Barnett BP, Bottomley PA, Bulte JW. Fluorine (¹⁹F) MRS and MRI in biomedicine. *NMR Biomed*. 2011; 24(2):114–129. [PubMed: 20842758]
16. Janjic JM, Ahrens ET. Fluorine-containing nanoemulsions for MRI cell tracking. *Wiley Interdiscip Rev Nanomed Nanobiotechnol*. 2009; 1(5):492–501. [PubMed: 19920872]
17. Ratner AV, Hurd R, Muller HH, Bradley-Simpson B, Pitts W, Shibata D, Sotak C, Young SW. ¹⁹F magnetic resonance imaging of the reticuloendothelial system. *Magn Reson Med*. 1987; 5(6):548–554. [PubMed: 3437815]
18. Giraudeau C, Flament J, Marty B, Boumezbeur F, Meriaux S, Robic C, Port M, Tsapis N, Fattal E, Giacomini E, Lethimonnier F, Le Bihan D, Valette J. A new paradigm for high-sensitivity F-19 magnetic resonance imaging of perfluorooctylbromide. *Magn Reson Med*. 2010; 63(4):1119–1124. [PubMed: 20373415]
19. Janjic JM, Srinivas M, Kadayakkara DK, Ahrens ET. Self-delivering nanoemulsions for dual fluorine-19 MRI and fluorescence detection. *J Am Chem Soc*. 2008; 130(9):2832–2841. [PubMed: 18266363]
20. Morel, PM.; Srinivas, M.; Turner, MS.; Fuschioti, P.; Munschi, R.; Baha, I.; Feili-Hariri, M.; Ahrens, ET. Dendritic cells that prevent diabetes in NOD mice express a unique pattern of chemokines that alter the migration of autoreactive T cells. 2009.
21. Srinivas M, Turner MS, Janjic JM, Morel PA, Laidlaw DH, Ahrens ET. In vivo cytometry of antigen-specific T cells using ¹⁹F MRI. *Magn Reson Med*. 2009; 62(3):747–753. [PubMed: 19585593]
22. Gerhardt GE, Lagow RJ. Synthesis of the perfluoropoly(ethylene glycol) ethers by direct fluorination. *J Org Chem*. 1978; 43(23):4505–4509.
23. Lowe KC. Engineering blood: Synthetic substitutes from fluorinated compounds. *J Tissue Eng*. 2003; 9(3):389–399.
24. Waiczies H, Lepore S, Janitzek N, Hagen U, Seifert F, Ittermann B, Purfurst B, Pezzutto A, Paul F, Niendorf T, Waiczies S. Perfluorocarbon particle size influences magnetic resonance signal and immunological properties of Dendritic Cells. *PLoS ONE*. 2011; 6(7)
25. Janjic, J.; Ahrens, ET. USPTO. 2008. Compositions and methods for producing cellular labels for nuclear magnetic resonance techniques. 60/959135
26. Neubauer AM, Myerson J, Caruthers SD, Hockett FD, Winter PM, Chen JJ, Gaffney PJ, Robertson JD, Lanza GM, Wickline SA. Gadolinium-modulated F-19 signals from perfluorocarbon

- nanoparticles as a new strategy for molecular imaging. *Magn Reson Med*. 2008; 60(5):1066–1072. [PubMed: 18956457]
27. Kok MB, de Vries A, Abdurrachim D, Prompers JJ, Grull H, Nicolay K, Strijkers GJ. Quantitative H-1 MRI, F-19 MRI, and F-19 MRS of cell-internalized perfluorocarbon paramagnetic nanoparticles. *Contrast Media & Molecular Imaging*. 2011; 6(1):19–27. [PubMed: 20648660]
 28. Tadros T, Izquierdo P, Esquena J, Solans C. Formation and stability of nano-emulsions. *Adv Colloid Interface Sci*. 2004; 108–109:303–318.
 29. Taylor P. Ostwald ripening in emulsions. *Adv Colloid Interface Sci*. 1998; 75(2):107–163.
 30. Freire MG, Dias AMA, Coelho MAZ, Coutinho JAP, Marrucho IM. Aging mechanisms of perfluorocarbon emulsions using image analysis. *J Colloid Interface Sci*. 2005; 286(1):224–232. [PubMed: 15848420]
 31. Postel M, Riess JG, Weers JG. Fluorocarbon emulsions - The stability issue. *Artif Cells Blood Substit Immobil Biotechnol*. 1994; 22(4):991–1005. [PubMed: 7849970]
 32. Kabalnov AS, Shchukin ED. Ostwald ripening theory. Applications to fluorocarbon emulsion stability. *Adv Colloid Interface Sci*. 1992; 38:69–97.
 33. Bible E, Dell'Acqua F, Solanky B, Balducci A, Crapo PM, Badylak SF, Ahrens ET, Modo M. Non-invasive imaging of transplanted human neural stem cells and ECM scaffold remodeling in the stroke-damaged rat brain by F-19- and diffusion-MRI. *Biomaterials*. 2012; 33(10):2858–2871. [PubMed: 22244696]
 34. Hitchens TK, Ye Q, Eytan DF, Janjic JM, Ahrens ET, Ho C. 19F MRI detection of acute allograft rejection with in vivo perfluorocarbon labeling of immune cells. *Magn Reson Med*. 2011; 65(4): 1144–1153. [PubMed: 21305593]
 35. Lim YT, Noh YW, Kwon JN, Chung BH. Multifunctional perfluorocarbon nanoemulsions for F-19-based magnetic resonance and near-infrared optical imaging of dendritic cells. *Chem Commun*. 2009; (45):6952–6954.
 36. Ahrens ET, Flores R, Xu HY, Morel PA. In vivo imaging platform for tracking immunotherapeutic cells. *Nat Biotechnol*. 2005; 23(8):983–987. [PubMed: 16041364]
 37. O'Hanlon CE, Amede KG, O'Hear MR, Janjic JM. NIR-labeled perfluoropolyether nanoemulsions for drug delivery and imaging. *J Fluor Chem*. 2012; 137:27–33. [PubMed: 22675234]
 38. Bulte JWM, Arbab AS, Douglas T, Frank JA. Preparation of magnetically labeled cells for cell tracking by magnetic resonance imaging. *Meth Enzymology*. 2004; 386:275–299.
 39. Bulte JWM, Kraitchman DL. Iron oxide MR contrast agents for molecular and cellular imaging. *NMR Biomed*. 2004; 17(7):484–499. [PubMed: 15526347]
 40. Boehm-Sturm P, Mengler L, Wecker S, Hoehn M, Kallur T. In vivo tracking of human neural stem cells with 19F magnetic resonance imaging. *PLoS ONE*. 2011; 6(12):e29040. [PubMed: 22216163]
 41. Ruiz-Cabello J, Walczak P, Kedziorek DA, Chacko VP, Schmieder AH, Wickline SA, Lanza GM, Bulte JW. In vivo “hot spot” MR imaging of neural stem cells using fluorinated nanoparticles. *Magn Reson Med*. 2008; 60(6):1506–1511. [PubMed: 19025893]
 42. Partlow KC, Chen JJ, Brant JA, Neubauer AM, Meyerrose TE, Creer MH, Nolte JA, Caruthers SD, Lanza GM, Wickline SA. F-19 magnetic resonance imaging for stem/progenitor cell tracking with multiple unique perfluorocarbon nanobeacons. *Faseb J*. 2007; 21(8):1647–1654. [PubMed: 17284484]
 43. Kadayakkara DK, Janjic JM, Pusateri LK, Young WB, Ahrens ET. In vivo observation of intracellular oximetry in perfluorocarbon-labeled glioma cells and chemotherapeutic response in the CNS using fluorine-19 MRI. *Magn Reson Med*. 2010; 64(5):1252–1259. [PubMed: 20860007]
 44. Helfer BM, Balducci A, Nelson AD, Janjic JM, Gil RR, Kalinski P, De Vries IJM, Ahrens ET, Mailliard RB. Functional assessment of human dendritic cells labeled for in vivo F-19 magnetic resonance imaging cell tracking. *Cytotherapy*. 2010; 12(2):238–250. [PubMed: 20053146]
 45. Helfer BM, Balducci A, Sadeghi Z, O'Hanlon C, Hijaz A, Flask CA, Wesa A. F-19 tracer preserves in vitro and in vivo properties of hematopoietic stem cells. *Cell Transplant*. 2012 Aug 2. [Epub ahead of print].
 46. Genove G, DeMarco U, Xu HY, Goins WF, Ahrens ET. A new transgene reporter for in vivo magnetic resonance imaging. *Nat Med*. 2005; 11(4):450–454. [PubMed: 15778721]

47. Iordanova B, Ahrens ET. In vivo magnetic resonance imaging of ferritin-based reporter visualizes native neuroblast migration. *Neuroimage*. 2012; 59(2):1004–1012. [PubMed: 21939774]
48. Cohen B, Dafni H, Meir G, Harmelin A, Neeman M. Ferritin as an endogenous MRI reporter for noninvasive imaging of gene expression in C6 glioma tumors. *Neoplasia*. 2005; 7(2):109–117. [PubMed: 15802016]
49. Gilad AA, McMahon MT, Walczak P, Winnard PT, Raman V, van Laarhoven HWM, Skoglund CM, Bulte JWM, van Zijl PCM. Artificial reporter gene providing MRI contrast based on proton exchange. *Nat Biotechnol*. 2007; 25(2):217–219. [PubMed: 17259977]
50. Dover R, Jayaram Y, Patel K, Chinery R. P53 expression in cultured-cells following radioisotope labeling. *J Cell Sci*. 1994; 107:1181–1184. [PubMed: 7929627]
51. Srivastava SC, Chervu LR. Radionuclide-labeled red-blood-cells - Current status and future prospects. *Semin Nucl Med*. 1984; 14(2):68–82. [PubMed: 6233700]
52. Barth RF, Singla O, Gillespi Gy. Use of Tc-99m as a radioisotopic label to study migratory patterns of normal and neoplastic-cells. *J Nucl Med*. 1974; 15(8):656–661. [PubMed: 4841819]
53. Gabay C, Kushner I. Mechanisms of disease: Acute-phase proteins and other systemic responses to inflammation. *New Engl J Med*. 1999; 340(6):448–454. [PubMed: 9971870]
54. Gordon S, Taylor PR. Monocyte and macrophage heterogeneity. *Nat Rev Immunol*. 2005; 5(12):953–964. [PubMed: 16322748]
55. Hertlein T, Sturm V, Kircher S, Basse-Lusebrink T, Haddad D, Ohlsen K, Jakob P. Visualization of abscess formation in a murine thigh infection model of staphylococcus aureus by F-19-magnetic resonance imaging (MRI). *PLoS ONE*. 2011; 6(3)
56. Ebner B, Behm P, Jacoby C, Burghoff S, French BA, Schrader J, Flögel U. Early assessment of pulmonary inflammation by (19)F MRI in vivo. *Circ Cardiovasc Imaging*. 2010; 3(2):202–U109. [PubMed: 20061515]
57. Flögel U, Ding Z, Hardung H, Jander S, Reichmann G, Jacoby C, Schubert R, Schrader J. In vivo monitoring of inflammation after cardiac and cerebral ischemia by fluorine magnetic resonance imaging. *Circulation*. 2008; 118(2):140–148. [PubMed: 18574049]
58. Weise G, Basse-Lusebrink TC, Kleinschnitz C, Kampf T, Jakob PM, Stoll G. In vivo imaging of stepwise vessel occlusion in cerebral photothrombosis of mice by F-19 MRI. *PLoS ONE*. 2011; 6(12)
59. Balducci A, Helfer BM, Ahrens ET, O'Hanlon CF, Wesa AK. Visualizing arthritic inflammation and therapeutic response by fluorine-19 magnetic resonance imaging (F-19 MRI). *J Inflamm*. 2012; 9:24.
60. Weise G, Basse-Lusebrink TC, Wessig C, Jakob PM, Stoll G. In vivo imaging of inflammation in the peripheral nervous system by (19)F MRI. *Exp Neurol*. 2011; 229(2):494–501. [PubMed: 21459088]
61. Flögel U, Su S, Kreideweiss I, Ding Z, Galbarz L, Fu J, Jacoby C, Witzke O, Schrader J. Noninvasive detection of graft rejection by in vivo 19F MRI in the early stage. *Am J Transplant*. 2011; 11(2):235–244. [PubMed: 21214858]
62. Noth U, Morrissey SP, Deichmann R, Jung S, Adolf H, Haase A, Lutz J. Perfluoro-15-crown-5-ether labelled macrophages in adoptive transfer experimental allergic encephalomyelitis. *Artif Cell Blood Sub*. 1997; 25(3):243–254.
63. Ratner AV, Muller HH, Bradley-Simpson B, Johnson DE, Hurd RE, Sotak C, Young SW. Detection of tumors with 19F magnetic resonance imaging. *Invest Radiol*. 1988; 23(5):361–364. [PubMed: 3384616]
64. Ratner AV, Muller HH, Bradley-Simpson B, Hirst D, Pitts W, Young SW. Detection of acute radiation damage to the spleen in mice by using fluorine-19 MR imaging. *Am J Roentgenol*. 1988; 151(3):477–480. [PubMed: 3261505]
65. Temme S, Bonner F, Schrader J, Flögel U. 19F magnetic resonance imaging of endogenous macrophages in inflammation. *WIREs Nanomed Nanobiotechnol*. 2012; 4(3):329–343.
66. Stoll G, Basse-Lusebrink T, Weise G, Jakob P. Visualization of inflammation using 19F-magnetic resonance imaging and perfluorocarbons. *WIREs Nanomed Nanobiotechnol*. 2012; 4(4):438–447.

67. Bonetto F, Srinivas M, Heerschap A, Mailliard R, Ahrens ET, Figdor CG, de Vries IJM. A novel (19)F agent for detection and quantification of human dendritic cells using magnetic resonance imaging. *Int J Cancer*. 2011; 129(2):365–373. [PubMed: 20839261]
68. Hu LZ, Hockett FD, Chen JJ, Zhang L, Caruthers SD, Lanza GM, Wickline SA. A Generalized strategy for designing F-19/H-1 dual-frequency MRI coil for small animal imaging at 4. 7 Tesla. *J Magn Reson Imaging*. 2011; 34(1):245–252. [PubMed: 21698714]
69. Hockett FD, Wallace KD, Schmieder AH, Caruthers SD, Pham CTN, Wickline SA, Lanza GM. Simultaneous dual frequency H-1 and F-19 open coil imaging of arthritic rabbit knee at 3T. *IEEE Trans Med Imaging*. 2011; 30(1):22–27. [PubMed: 20699209]
70. Mispelter, J.; Lupu, M.; Briguet, A. NMR probeheads for biophysical and biomedical experiments. London: Imperial College; 2006.
71. Hayward, W. Introduction to radio frequency design. Upper Saddle River: Prentice-Hall; 1982.
72. van Heeswijk RB, Pilloud Y, Flögel U, Schwitter J, Stuber M. Fluorine-19 magnetic resonance angiography of the mouse. *Plos ONE*. 2012; 7(7):e42236. [PubMed: 22848749]
73. Keupp J, Rahmer J, Grasslin I, Mazurkewitz PC, Schaeffter T, Lanza GM, Wickline SA, Caruthers SD. Simultaneous dual-nuclei imaging for motion corrected detection and quantification of 19F imaging agents. *Magn Reson Med*. 2011; 66(4):1116–1122. [PubMed: 21394779]
74. Zhao D, Jiang L, Hahn EW, Mason RP. Comparison of 1H blood oxygen level-dependent (BOLD) and 19F MRI to investigate tumor oxygenation. *Magn Reson Med*. 2009; 62(2):357–364. [PubMed: 19526495]
75. Dardzinski BJ, Sotak CH. Rapid tissue oxygen tension mapping using 19F inversion-recovery echo- planar imaging of perfluoro-15-crown-5-ether. *Magn Reson Med*. 1994; 32(1):88–97. [PubMed: 8084241]
76. Griswold MA, Jakob PM, Heidemann RM, Nittka M, Jellus V, Wang JM, Kiefer B, Haase A. Generalized autocalibrating partially parallel acquisitions (GRAPPA). *Magnet Reson Med*. 2002; 47(6):1202–1210.
77. Pruessmann KP, Weiger M, Scheidegger MB, Boesiger P. SENSE: Sensitivity encoding for fast MRI. *Magnet Reson Med*. 1999; 42(5):952–962.
78. Kim YC, Narayanan SS, Nayak KS. Accelerated three-dimensional upper airway MRI using compressed sensing. *Magn Reson Med*. 2009; 61(6):1434–1440. [PubMed: 19353675]
79. Liang D, Liu B, Wang JJ, Ying L. Accelerating SENSE using compressed sensing. *Magn Reson Med*. 2009; 62(6):1574–1584. [PubMed: 19785017]
80. Schirra CO, Weiss S, Krueger S, Pedersen SF, Razavi R, Schaeffter T, Kozerke S. Toward true 3D visualization of active catheters using compressed sensing. *Magn Reson Med*. 2009; 62(2):341–347. [PubMed: 19526499]
81. Ajraoui S, Lee KJ, Deppe MH, Parnell SR, Parra-Robles J, Wild JM. Compressed sensing in hyperpolarized He-3 lung MRI. *Magn Reson Med*. 2010; 63(4):1059–1069. [PubMed: 20373407]
82. Kampf T, Fischer A, Basse-Lusebrink TC, Ladewig G, Breuer F, Stoll G, Jakob PM, Bauer WR. Application of compressed sensing to in vivo 3D F-19 CSI. *J Magn Reson*. 2010; 207(2):262–273. [PubMed: 20932790]
83. Yerly J, Lauzon ML, Chen HS, Frayne R. A simulation-based analysis of the potential of compressed sensing for accelerating passive mr catheter visualization in endovascular therapy. *Magn Reson Med*. 2010; 63(2):473–483. [PubMed: 20099327]
84. Zhong J, Mills PH, Hitchens TK, Ahrens ET. Accelerated fluorine-19 MRI cell tracking using compressed sensing. *Magn Reson Med*. 2012 (in press).
85. Gudbjartsson H, Patz S. The Rician distribution of noisy MRI data. *Magn Reson Med*. 1995; 34(6): 910–914. [PubMed: 8598820]
86. Robson MD, Gatehouse PD, Bydder M, Bydder GM. Magnetic resonance: An introduction to ultrashort TE (UTE) imaging. *J Comput Assist Tomogr*. 2003; 27(6):825–846. [PubMed: 14600447]
87. Idiyatullin D, Corum C, Park JY, Garwood M. Fast and quiet MRI using a swept radiofrequency. *J Magn Reson*. 2006; 181(2):342–349. [PubMed: 16782371]
88. Pipe JG. Motion correction with PROPELLER MRI: Application to head motion and free-breathing cardiac imaging. *Magn Reson Med*. 1999; 42(5):963–969. [PubMed: 10542356]

89. Stehning C, Bornert P, Nehrke K, Eggers H, Stuber M. Free-breathing whole-heart coronary MRA with 3D radial SSFP and self-navigated image reconstruction. *Magnet Reson Med*. 2005; 54(2): 476–480.
90. Guo Q, Mattrey RF, Guclu C, Buxton RB, Nalcioğlu O. Monitoring of pO₂ by spin-spin relaxation rate 1/T₂ of ¹⁹F in a rabbit abscess model. *Artif Cells Blood Substit Immobil Biotechnol*. 1994; 22(4):1449–1454. [PubMed: 7849956]
91. Yu JX, Kodibagkar VD, Cui W, Mason RP. ¹⁹F: A versatile reporter for non-invasive physiology and pharmacology using magnetic resonance. *Curr Med Chem*. 2005; 12(7):819–848. [PubMed: 15853714]
92. Mason RP, Shukla H, Antich PP. In vivo oxygen tension and temperature: Simultaneous determination using ¹⁹F NMR spectroscopy of perfluorocarbon. *Magn Reson Med*. 1993; 29(3): 296–302. [PubMed: 8450738]
93. Mason RP, Hunjan S, Constantinescu A, Song Y, Zhao D, Hahn EW, Antich PP, Peschke P. Tumor oximetry: Comparison of ¹⁹F MR EPI and electrodes. *Adv Exp Med Biol*. 2003; 530:19–27. [PubMed: 14562701]
94. Zhao D, Jiang L, Mason RP. Measuring changes in tumor oxygenation. *Methods enzymol*. 2004; 386:378–418. [PubMed: 15120262]
95. Sotak CH, Hees PS, Huang HN, Hung MH, Krespan CG, Raynolds S. A new perfluorocarbon for use in fluorine-19 magnetic resonance imaging and spectroscopy. *Magn Reson Med*. 1993; 29(2): 188–195. [PubMed: 8429782]
96. Mason RP, Nunnally RL, Antich PP. Tissue oxygenation - a novel determination using F-19 surface coil nmr-spectroscopy of sequestered perfluorocarbon emulsion. *Magn Reson Med*. 1991; 18(1):71–79. [PubMed: 2062243]
97. Hees PS, Sotak CH. Assessment of changes in murine tumor oxygenation in response to nicotinamide using ¹⁹F NMR relaxometry of a perfluorocarbon emulsion. *Magn Reson Med*. 1993; 29(3):303–310. [PubMed: 8450739]
98. Mason RP, Antich PP, Babcock EE, Constantinescu A, Peschke P, Hahn EW. Non-invasive determination of tumor oxygen tension and local variation with growth. *Int J Radiat Oncol Biol Phys*. 1994; 29(1):95–103. [PubMed: 8175452]
99. van der Sanden BP, Heerschap A, Simonetti AW, Rijken PF, Peters HP, Stuben G, van der Kogel AJ. Characterization and validation of noninvasive oxygen tension measurements in human glioma xenografts by ¹⁹F-MR relaxometry. *Int J Radiat Oncol Biol Phys*. 1999; 44(3):649–658. [PubMed: 10348296]
100. Cohn SM. Oxygen therapeutics in trauma and surgery. *J Trauma*. 2003; 54(5):S193–S198. [PubMed: 12768124]
101. Caruthers SD, Neubauer AM, Hockett FD, Lamerichs R, Winter PM, Scott MJ, Gaffney PJ, Wickline SA, Lanza GM. In vitro demonstration using ¹⁹F magnetic resonance to augment molecular imaging with paramagnetic perfluorocarbon nanoparticles at 1.5 Tesla. *Invest Radiol*. 2006; 41(3):305–312. [PubMed: 16481914]

**Fig. 1.**

In vivo cytometry examples using *ex vivo* PFC labeled cells in rodent models. ^{19}F images of the labeled cells are displayed on a 'hot-iron' intensity scale, and the anatomical (^1H) images are shown in grayscale. **(a)** Composite image through the torso following intravenous inoculation with labeled DCs. Cells are apparent in the liver, spleen, and weakly in the lungs (36). **(b)** Adoptively transferred T cells selectively home to the pancreas in a pre-diabetic mouse model. Activated T cells bearing receptors specific for an islet antigen were PFC labeled and then transferred (5×10^6 cells) into an NOD SCID mouse (1). The image shows T cells (pseudo-color) homing to the pancreas (P). **(c)** Neuronal stem cells injected into the infarct of a rat stroke model (33). A ^{19}F reference capillary is outside the brain.

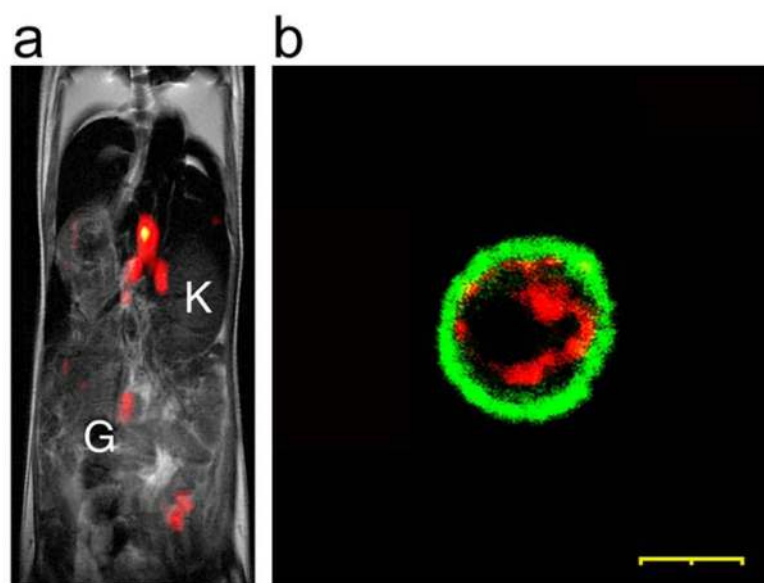


Fig. 2.

Dual-mode ^{19}F MRI-fluorescent PFC emulsion (19). **(a)** Shows CD4+ T cells from a wild-type DBA mouse, labeled *ex vivo*, and infused back into a recipient of the same strain. The *in vivo* ^{19}F image (pseudo-color) through the torso shows a localized accumulation of T cells in periaortic lymph nodes. The ^1H image is in grayscale, and the kidneys (K) and gut (G) are noted. **(b)** Fluorescence microscopy shows intracytoplasmic localization of PFC-dye (BODIPY, red) in mouse T cells, where the nucleus is blue (Hoechst dye) and the cell surface is stained with CD4- FITC antibody (green). (Scale bar is 20 μm)

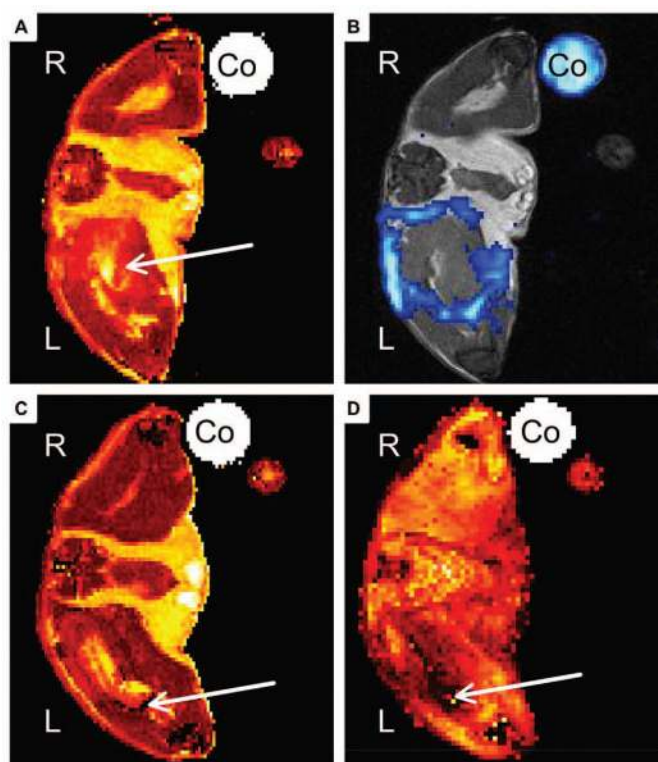


Fig. 3.

MRI of inflammation using *in situ* macrophage labeling in a mouse model of acute soft-tissue infection (55). Panels (A) and (B) shows images at day 2 post infection showing regions of macrophage burden in thigh. Images were acquired 24 hours after *in situ* PFC administration. (A) Displays ^1H T_2 map, where hyperintensity is clearly observed at site of muscle infection (arrow). (B) Shows ^{19}F CSI overlay (blue) on anatomical ^1H image (grayscale), where the ^{19}F image shows pronounced accumulation of PFC at the rim of abscess area. Panels (C) and (D) show same mouse model infused with iron-oxide nanoparticles with same timing as above. (C) Displays ^1H T_2 map and shows diffuse hyperintense region at site of infection (arrow). Panel (D) is a T_2^* -weighted image that shows diffusely distributed susceptibility effects in the infected muscle (arrow). (“Co” is capillary tube filled with PFC dilution, “R” is right side, and “L” is left side of mouse).

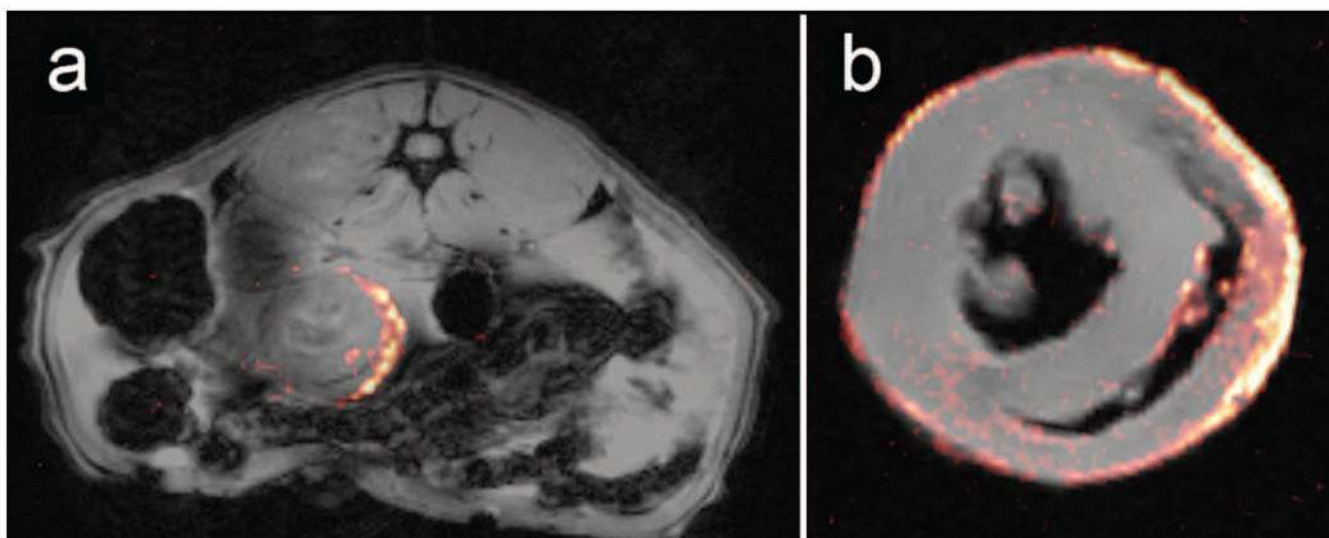


Fig. 4.

In situ PFC labeling detects macrophage infiltration in a heterotopic myocardium transplantation model (34). A working *en bloc* donor heart and lung from DA rat was transplanted to a recipient BN rat abdomen (day 0), leaving the native heart intact. At day 5 an intravenous injection of PFC was given, and 24 hours later a composite *in vivo* $^{19}\text{F}/^1\text{H}$ image (**a**) displays macrophage infiltration in the allograft myocardium (^{19}F is hot-iron pseudo-color). The native heart shows no ^{19}F signal (data not shown). Images were acquired in about 20 min at 7 T using a conventional gradient-echo sequence [data acquisition details given in Ref. (34)]. (**b**) ^{19}F signal in the myocardium was confirmed using high resolution *ex vivo* MRI of the fixed heart.

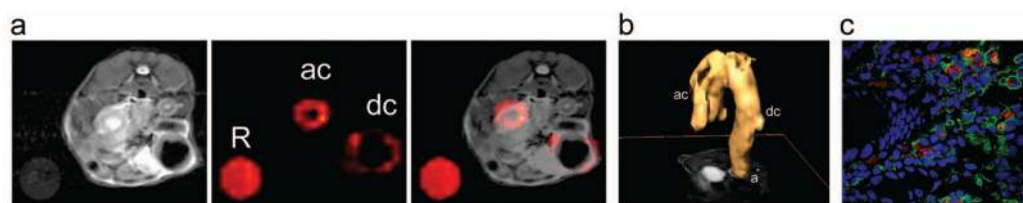


Fig. 5.

Inflammatory bowel disease (IBD) in an IL-10^{-/-} mouse model visualized using *in situ* PFC labeling and ^{19}F MRI (4). The $^1\text{H}/^{19}\text{F}$ MRI reveals PFC distribution in colon walls in a representative IBD mouse. **(A)** *In vivo* axial slices through the abdomen of a single mouse shows PFC accumulation in the ascending (ac) and descending colon (dc) in a mouse two days post-injection. The left panel shows ^1H images (grayscale), the middle panel shows corresponding ^{19}F images (pseudocolor), and the right panel shows composite $^1\text{H}/^{19}\text{F}$ images. “R” represents a reference tube alongside the torso containing PFC emulsion. Panel **(B)** is a 3D rendering of the *in vivo* ^{19}F MRI data from the abdomen in the IL-10^{-/-} mice; substantial inflammation in the ascending and descending colon is apparent. Here, “ac” = ascending colon, “dc” = descending colon and “a” = anus. No manual image segmentation is used to make rendering, just noise thresholding of the ^{19}F data. Panel **(C)** shows that macrophage burden forms the basis of ^{19}F signal in the colon. Data is immunohistochemistry of the colon in IL-10^{-/-} mice and shows that PFC labeled with DiI (red) (3) is localized within the macrophages (F4/80, green) at 2 days. Nuclei are stained with Hoechst 33342 (blue). The same study shows that PFC-DiI does not colocalize with ly6c positive cells or endothelial cells (data not shown).

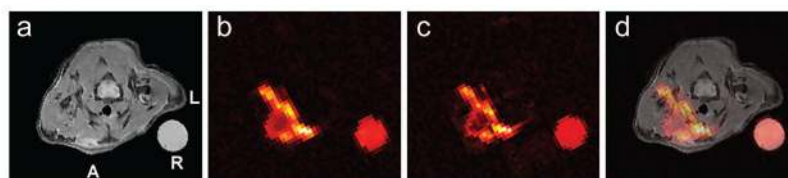
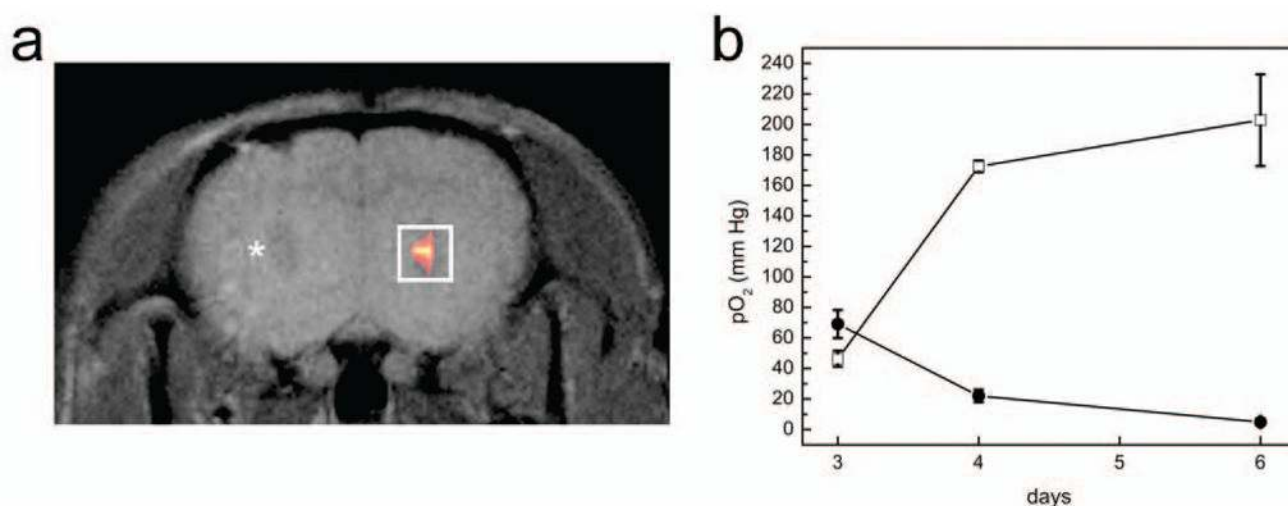


Fig. 6.

Compressed sensing 3D data acquisition schemes can accelerate ^{19}F cell tracking studies. A pseudorandom CS undersampling schemes emphasizing the k-space center was used, with an acceleration factor (AF) of 8-fold (84). Undersampling occurs in the two phase encoding directions (matrix size 128×128), whereas in the readout direction the k-space remains fully sampled. Panels (a–d) show *in vivo* ^{19}F 3D CS-RARE images in a localized inflammation mouse model (84). The pseudo-colored images show macrophage (PFC) accumulation in the region of wounding-induced inflammation. Panel (a) shows a T_2 -weighted anatomical ^1H image. Panel (b) is a single slice from a 3D ^{19}F CS-RARE image with AF=8 and 8 averages. Panel (c) is an AF=1 (fully-sampled k-space) RARE image with 8 averages. (d) Displays a $^1\text{H}/^{19}\text{F}$ fused image of (a+b). The PFC emulsion was injected 24 hours after injury and imaged at 72 hours. Here, A=anterior wall, L=left, and R= reference.

**Fig. 7.**

In vivo ^{19}F MRI and pO_2 sensing in rat brain glioma (43). **(a)** A composite $^{19}\text{F}/^1\text{H}$ image of the labeled 9L glioma cells stereotactically injected into the right striatum three days prior. The ^{19}F is rendered in a hot-iron intensity scale and the ^1H is grayscale. The white rectangular box encompassing the ^{19}F signal represents the approximate voxel placement for MRS. Panel **(b)** shows the longitudinal pO_2 changes after BCNU treatment. Post-BCNU, the pO_2 increase persists for at least 72 hours (day 6). In controls, pO_2 gradually decreased from day 3 to day 6 (closed circles).